

# ICE GENESIS

## Creating the next generation of 3D simulation means for icing

Type of action: Research and Innovation Action

Call identifier: H2020-MG-2018-SingleStage

Topic: MG-2-5-2018 Innovative technologies for improving aviation safety and certification in icing conditions

### Deliverable D6.5

## Assessment of FZRA capabilities for each IWT involved in the project

EC Grant Agreement number:

824310

Start date of project: 1 January 2019

Duration: 60 months

Lead beneficiary of this deliverable:

CIRA

Due date of deliverable: 31/10/2022

Actual submission date: 31/07/2024

Version #: R1.3

Project funded by the European Commission within the H2020 Programme (2014-2020)		
Type		
R	Document, report excluding the periodic and final reports	X
DEM	Demonstrator, pilot, prototype	
DEC	Websites, patents filing, press & media actions, videos, etc.	
OTHER	Software, technical diagram, etc.	
ETHICS	Ethics requirement	
ORDP	Open Research Data Pilot	
Dissemination level		
PU	PUBLIC, fully open, no embargo e.g. web	X
PU+E1	PUBLIC after embargo of 12 months from date of publication	
PU+E3	PUBLIC after embargo of 3 years after the project's end	
RE	RESTRICTED, only for certain members of the consortium (including the Commission Services):	
CO	CONFIDENTIAL, only for members of the consortium (including the Commission Services)	
CO+IGAB	CONFIDENTIAL, only for members of the consortium (including the Commission Services) and for the ICE GENESIS Advisory Board	

## Revision History

V #	Date	Description / Reason of change	Author
1.0	17.05.2022	First Version	W. Breitfuß (RTA)
1.1	09.02.2024	Last version includes CIRA contribution	B. Esposito (CIRA)
1.2	15.02.2024	Updated RTA part	W. Breitfuß (RTA)
1.3	16.02.2024	Reviewed Version	W. Breitfuß (RTA)

## Deliverable Contributors

### Authors

Organisation	Authors' name	Export control status date	Export control status
RTA	Wolfgang Breitfuß	16/02/2024	No data subject to export control

### Contributors

Organisation	Authors' name	Export control status date	Export control status
CIRA	Biagio Esposito	16/02/2024	No data subject to export control
CU	Hugo Pervier	16/02/2024	No data subject to export control
DLR	Romy Heller	16/02/2024	No data subject to export control
RV	Sawitree Saengkaew	16/02/2024	No data subject to export control

### Export Control Status

Author / Contributor	Type of data	Position in document of concerned text/data*	Jurisdiction and ECCN under this jurisdiction	Status of authorization
RTA	Experimental data, Computational data, Scientific papers	§4, 6	No data subject to export control	N/A
CIRA	Experimental data	§5, 6	No data subject to export control	N/A
DLR	Experimental data	§4, 5, 6	No data subject to export control	N/A
CU	Experimental data	§4.5.1	No data subject to export control	N/A
RV	Experimental data	§4.2.3	No data subject to export control	N/A

**\*To be checked by the Owner of the document before delivery of the document!**

## Internal Reviewers

Organisation	Internal Reviewers' name
Airbus	Olivier Blesbois
Dassault Aviation	Francois Caminade

## Table of Contents

1	Glossary.....	5
2	Executive Summary.....	6
3	Introduction .....	7
4	FZRA Assessment at RTA.....	8
4.1	RTA IWT Configuration.....	8
4.2	Feasibility Study .....	8
4.2.1	Particle Trajectories and Secondary Droplet Breakup .....	8
4.2.2	Droplet Temperature .....	10
4.2.3	Droplet Temperature Validation.....	11
4.3	RTA Freezing Rain MVD > 40 $\mu\text{m}$ Calibration.....	13
4.4	MVD / PSD Measurements .....	14
4.4.1	MVD Calibration.....	14
4.4.2	PSD Calibration.....	15
4.5	LWC Measurements.....	18
4.5.1	LWC Calibration.....	18
4.5.2	LWC Uniformity.....	19
4.6	RTA FZRA Envelopes.....	21
5	CIRA-IWT .....	22
5.1.1	Preliminary assessment of FZRA with MVD>40 $\mu\text{m}$ in CIRA-IWT .....	23
6	Conclusion.....	25
7	References .....	26

## Table of Figures

Figure 1:	Schematic of the RTA IWT “high-speed configuration” .....	8
Figure 2:	Example particle tracks for FZRA droplets (100-1200 $\mu\text{m}$ ) in the RTA IWT at a test section airspeed of 30 m/s (left) and 80 m/s (right) .....	9
Figure 3:	Example secondary droplet breakup analysis for a 1500 $\mu\text{m}$ droplet in the RTA IWT at 80 m/s (dashed line = with droplet deformation, solid line = spherical model).....	10
Figure 4:	Example trajectory of a 1500 $\mu\text{m}$ droplet in the RTA IWT at 80 m/s (dashed line = with droplet deformation, solid line = spherical model) .....	10

Figure 5: Particle size distribution and mass averaged diameters used for the droplet temperature investigation.....	11
Figure 6: Results for a FZRA icing cloud simulation in the RTA IWT, the asterisks mark the position where the droplet reaches a supercooled state.....	11
Figure 7: Mean droplet temperature in the test section (12.5m from the spray nozzles) at the RTA IWT .....	11
Figure 8: Example of validated measurement at RTA (for air temperature = -5°C, air velocity = 60 m/s, fitted PSD (left), recorded rainbow image (right)).....	12
Figure 9: Appendix O Freezing Rain MVD > 40 µm PSD (left) and LWC range (right).....	13
Figure 10: Average Cumulative Mass Spectrum for FZRA MVD > 40 µm compared to each individual cumulative mass spectra [2, p.45] .....	13
Figure 11: Comparison of calibrated and measured MVDs versus test section airspeed for FZRA MVD > 40 µm .....	15
Figure 12: Measured PSDs for FZRA using the Malvern Spraytec compared to Appendix O requirements, cumulative volume (left), q - q plot (right); measurement performed at 2°C.....	16
Figure 13: Measured PSDs for FZRA using the FCDP/2D-S/PIP combination compared to Appendix O requirements, cumulative volume (left), q - q plot (right); measurement performed at -5°C.....	16
Figure 14: Measured PSDs for FZRA L1 using the FCDP/2D-S/PIP combination compared to Appendix O requirements, cumulative volume (left), q - q plot (right); measurement performed at 2°C .....	16
Figure 15: Calibrated PSD of FZRA L1 versus appendix O requirement, cumulative volume (left), q - q plot (right) .....	17
Figure 16: Comparison of measured cumulative volume versus prediction using the PSD calibration; Malvern measurements (left), FCDP/2D-S/PIP combination measured at -5°C (right).....	17
Figure 17: Comparison of measured cumulative volume versus prediction using the PSD calibration; FCDP/2D-S/PIP combination measured at 2°C .....	17
Figure 18: Comparison of calibrated and measured LWCs for FZRA MVD > 40 µm, full bi-modal distribution (left), only large mode (right).....	18
Figure 19: LWC Uniformity for “FZRA L1” at a test section airspeed of 60 m/s, measured using the ice accretion grid, in total 22 “SLD” Nozzles were used.....	19
Figure 20: Photographs of a FZRA MVD > 40 µm ice accretion (Setting “FZRA L1”), TAS = 60 m/s, SAT = -5°C, exposure duration = 600s.....	20
Figure 21 .....	21
Figure 22 .....	21
Figure 22: CIRA Icing Wind Tunnel layout with main information on the test section configurations and performance .....	22
Figure 23: DLR CCP (Cloud Combination Probe) installed in the centerline of the CIRA IWT test section during the PSD/MVD measurement slot. The picture on the left shows the droplet images with diameters higher than 100 µm .....	23
Figure 24: Typical plots representing some of the cloud conditions collected during the CCP measurements. In this particular case, the data have been collected at 110 m/s with airstream temperature at -6°C and pressure altitude representing 6,096 m. The plot on the top represents the combination of the concentration measured by each sensor (CDP+CIP-Gs); the plot on below shows the mass distribution for the combined PSD.....	24

## 1 Glossary

---

Abbreviation / Acronym	Description/meaning
2D-S	2-Dimensional Stereo Probe
CCP	Cloud Combination Probe
CIP	Cloud Imaging Probe
CPD	Cloud Droplet Probe
FCDP	Fast Cloud Droplet Probe
FZDZ	Freezing Drizzle
FZRA	Freezing Rain
IKP	Isokinetic Probe
LWC	Liquid Water Content
MVD	Median Volumetric Diameter
PIP	Precipitation Imaging Probe
PSD	Particle Size Distribution
SLD	Supercooled Large Droplet
TWC	Total Water Content

## 2 Executive Summary

---

This deliverable provides the results from the measurements and calibration activities performed in the RTA Icing Wind Tunnel (IWT) for Freezing Rain (FZRA) cloud conditions and a summary of the measurements at CIRA-IWT, showing a potential capability for FZRA cloud generation.

A full assessment of the FZRA capabilities for RTA-IWT has been presented in this report. The guidelines on the procedures to be followed for the cloud characterizations have been defined in deliverable D6.1-2, "Proposal of Calibration Instruments and Procedures for FZDZ and FZRA". Three separate test campaigns, starting in August 2019 and ending in June 2021, were conducted at RTA, whose SLD capabilities were already available at the start of the project, limited to PSD/MVD calibration for the FZDZ. During the project period, a better assessment of the LWC and a review of the PSD/MVD envelope for both FZDZ and FZRA were performed using selected instrumentation from Deliverable D6.1-2 to achieve a better accuracy of the LWC characterization. In addition, a refinement of the PSD/MVD, cloud uniformity, and droplet temperature measurements were performed and are presented in this report outlining the RTA-IWT calibration for freezing rain with an MVD greater than 40  $\mu\text{m}$ .

After the upgrade with a new spray nozzle, followed by the commissioning of the spray bar system in January-February 2022, the measurements in the CIRA-IWT were planned to a single slot from April 2022 to early June 2022. The calibration began with the cloud uniformity check and extended to LWC and PSD/MVD measurements for one of the three spray bar configurations. The time available was only allowed to characterize cloud conditions at the sea level for FZDZ higher and lower than 40  $\mu\text{m}$ , with few conditions for checking different pressure altitudes and spray bar configurations. FZRA conditions were not addressed during the available measurement slot, where the instrument configuration was focused only on FZDZ clouds, although some cloud conditions showed potential FZRA features in their spectra.

### 3 Introduction

---

The ambition of the ICE GENESIS project is to improve the experimental test capabilities of icing facilities to generate or reproduce representative Supercooled Large Droplet (SLD) conditions and to define a common calibration methodology. The performed measurements and calibration activities for Freezing Rain with an MVD of larger than 40 microns are summarized in this report, showing the basic calibration data for these conditions at the RTA Icing Wind Tunnel (IWT). A summary of potential capabilities for the CIRA-IWT is also provided.

## 4 FZRA Assessment at RTA

### 4.1 RTA IWT Configuration

All of the RTA tests and measurements mentioned in this report were performed in the large IWT using the high-speed configuration with the additional contraction nozzle, a schematic is shown in Figure 1. The test section area indicated in the schematic shows the calibrated area for Appendix C icing clouds. This setup enables test section airspeeds between 20 m/s and 80 m/s and offer the benefit of a low contraction ratio, which minimizes potential secondary droplet breakup. Furthermore, the asymmetric contraction nozzle also proved to be beneficial for the generation and transport of large rain droplets.

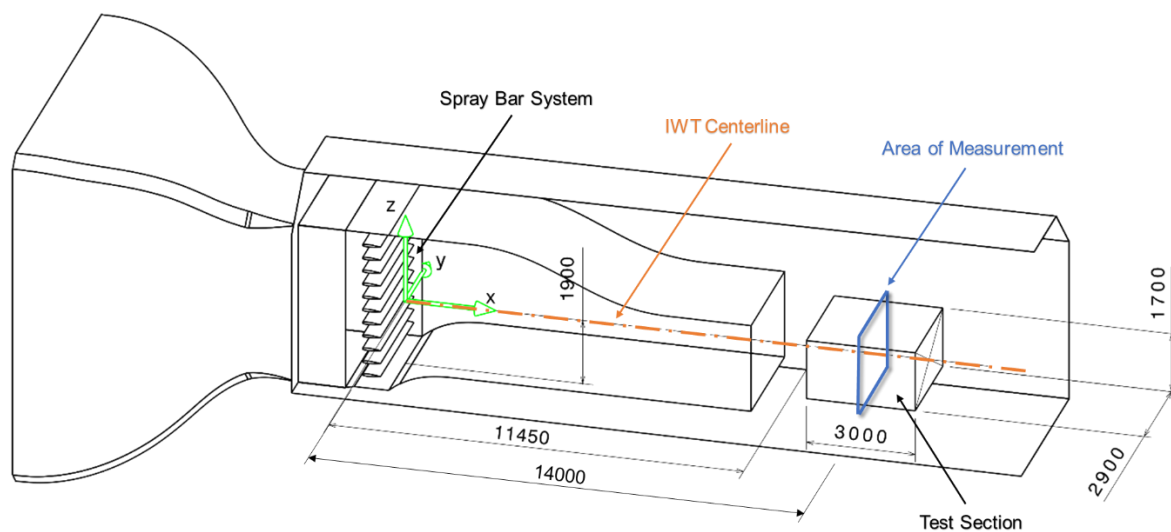


Figure 1: Schematic of the RTA IWT “high-speed configuration”

RTA’s spray bar system features eleven spray bars with 24 spray nozzles each. The 24 nozzles of each spray bar are split into two separately controllable circuits, where every second nozzle belongs to circuit 1 and every other nozzle to circuit 2. The supply water- and air-pressures as well as the water supply temperature can be controlled independently for those two circuits, which enables the generation of bimodal Particle Size Distributions (PSDs). The large particles can be injected with pre-cooled water, whereas the particles of the small mode can be supplied with pre-heated water in order to prevent freeze-out. The distance of about 11.5 m from the injection to the test section should provide sufficient time for the large droplets to cool down close to ambient temperature (see section 4.2.2).

### 4.2 Feasibility Study

A feasibility study was performed to investigate the potential of generating FZDZ and FZRA conditions in RTA’s IWT by means of spray nozzle assessments using a nozzle test rig, numerical simulations and preliminary tests in the IWT. These investigations were performed prior to the ICE GENESIS project and therefore are just summarised briefly in this report.

#### 4.2.1 Particle Trajectories and Secondary Droplet Breakup

The particle trajectories at different test section airspeeds were analysed using numerical simulation tools. The injection velocities of the particles as well as the spray cone angle were measured using a high-speed camera and used as an input for the simulations. The analysis revealed that for FZRA

conditions a minimum test section airspeed of 40 m/s to 45 m/s is required as the gravitational influence of the large rain droplets significantly affects the trajectories at low speeds. The results also showed that only certain spray bars could be used, as some of the large particles impinge on the additional contraction nozzle before reaching the test section. Example results for 100-1200  $\mu\text{m}$  droplets can be found in Figure 2.

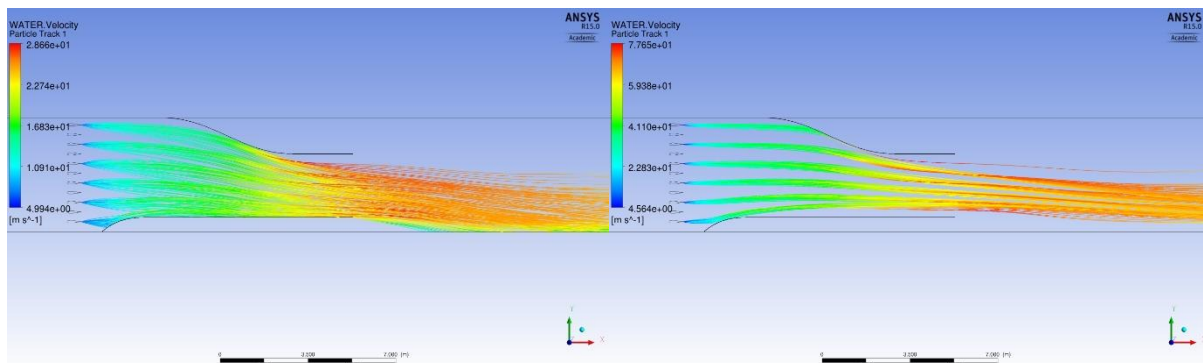


Figure 2: Example particle tracks for FZRA droplets (100-1200  $\mu\text{m}$ ) in the RTA IWT at a test section airspeed of 30 m/s (left) and 80 m/s (right)

Furthermore, potential secondary droplet breakup was analysed using the so-called Weber number. The critical Weber number for when breakup starts to occur varies between 11-14 [7]. Simulations with and without a droplet deformation model were performed. For the runs with deformation the same approach NASA used to investigate breakup in Glenn Icing Research Tunnel (IRT) was used [4]. The Droplet deformation is based on a modified Bond number from [5] and the drag of the deformed droplet was taken from [6]. The simulations have shown that droplets with diameters of up to about 1500  $\mu\text{m}$  can be transported to the test section at the maximum airspeed without exceeding a Weber number of 14, when the deformed droplet model is used. This can mainly be attributed to the low contraction ratio (1.84) of the additional contraction nozzle. In Figure 3 and Figure 4 an example evaluation for a rain droplet with a diameter of 1500  $\mu\text{m}$  is shown for the maximum airspeed of 80 m/s where the solid lines show the fully spherical model, and the dashed lines show the results using the droplet deformation model. A maximum Weber Number of 13.7 is reached (with the deformation model) in the main contraction zone of the additional contraction nozzle, where the flow is accelerated the most. In the test section the droplet is about 18% slower compared to the ambient airspeed and has a trajectory angle within less than  $0.6^\circ$  compared to a droplet falling with its terminal velocity at an airspeed of 80 m/s. The maximum achievable droplet size was later validated experimentally with PSD measurements in the IWT.

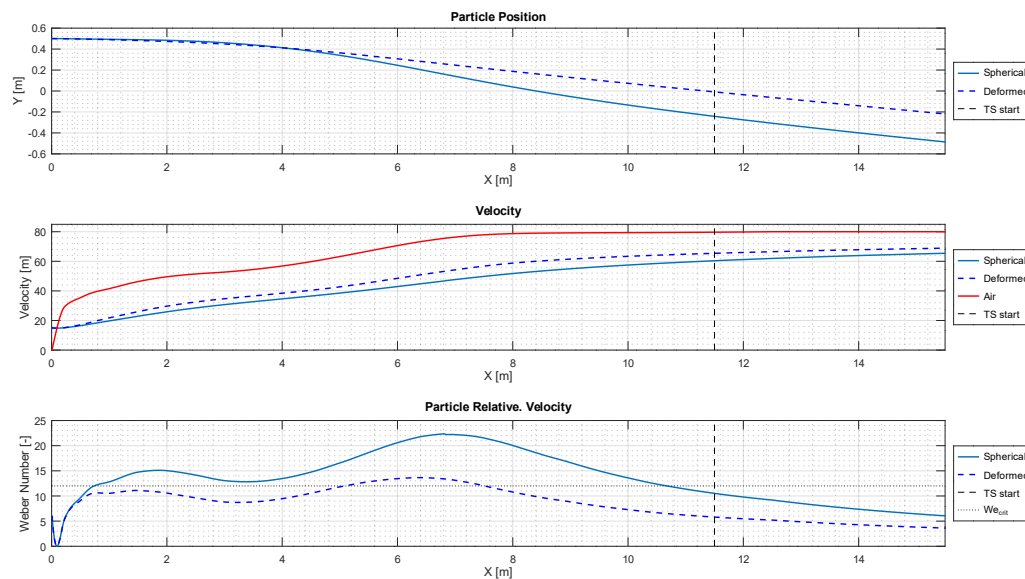


Figure 3: Example secondary droplet breakup analysis for a  $1500\ \mu\text{m}$  droplet in the RTA IWT at  $80\ \text{m/s}$  (dashed line = with droplet deformation, solid line = spherical model)

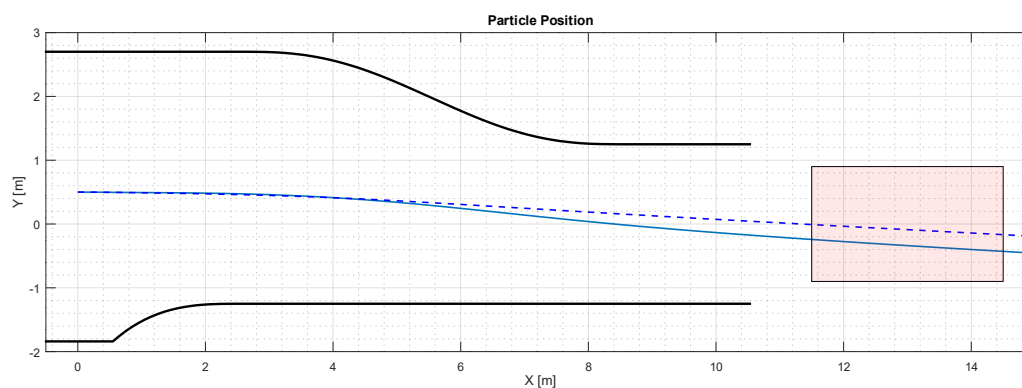


Figure 4: Example trajectory of a  $1500\ \mu\text{m}$  droplet in the RTA IWT at  $80\ \text{m/s}$  (dashed line = with droplet deformation, solid line = spherical model)

## 4.2.2 Droplet Temperature

The achievable droplet temperatures in the test section were also investigated by means of numerical and analytical simulations for various ambient conditions using the model described in [8]. The results for a FZRA MVD  $> 40\ \mu\text{m}$  condition, using the mass averaged diameters of the 11 bin calibrated PSD for the “FZRA L1” setting from section 4.4.2 (see Figure 5), at a static test section air temperature of  $-10^\circ\text{C}$  and a test section airspeed of  $60\ \text{m/s}$  are shown in Figure 6 and Figure 7. The increased thermal inertia of the droplets from the SLD spectrum causes a shallow cool down behaviour and therefore requires pre-cooled water at considerable low temperatures. The injection temperature of the droplets was set to  $2^\circ\text{C}$ , which is the expected droplet temperature at the exit of the spray nozzles (the measured water temperature in the spray bar is usually kept between  $4\text{--}6^\circ\text{C}$  for FZRA). Droplets above about  $800\ \mu\text{m}$  (which account for about 25% of the total mass) remained just above  $0^\circ\text{C}$ , with a maximum temperature of about  $1.3^\circ\text{C}$  for the largest size bin. The mass averaged temperature for the full spectrum was about  $-3.4^\circ\text{C}$ .

Running the same case at  $-13^\circ\text{C}$ , the mass averaged temperature ended up at about  $-4.8^\circ\text{C}$ , with a maximum temperature of  $1.1^\circ\text{C}$ . At an ambient temperature of  $-2^\circ\text{C}$  the mass averaged temperature would be about  $0.2^\circ\text{C}$ , with a maximum temperature of  $1.75^\circ\text{C}$ .

The simulations have shown, that the achievable droplet temperatures for the largest size bin is between about 4°C and 12°C warmer compared to the ambient temperature. The mass averaged temperature remains within less than 10°C when the water injection temperature is as cold as 2°C .

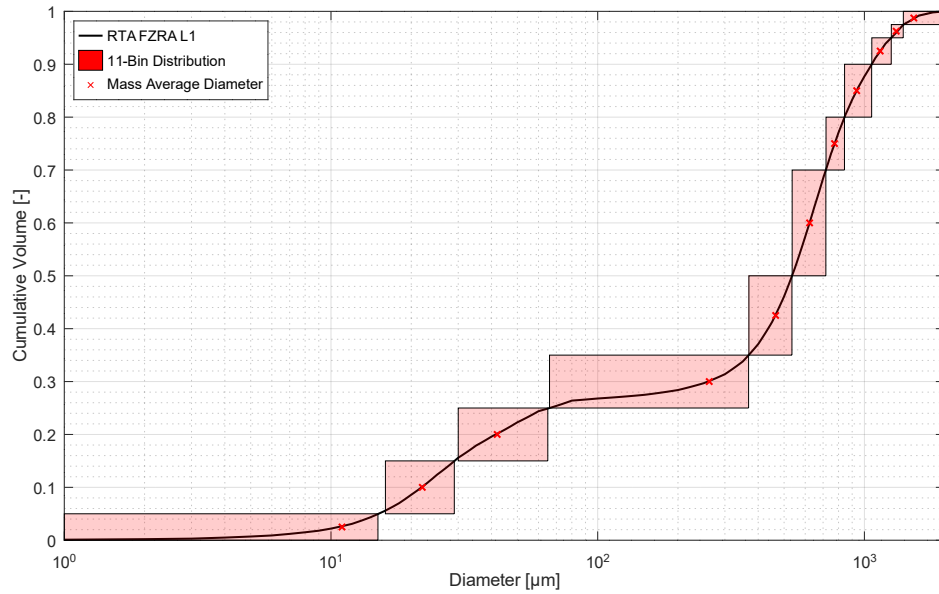


Figure 5: Particle size distribution and mass averaged diameters used for the droplet temperature investigation

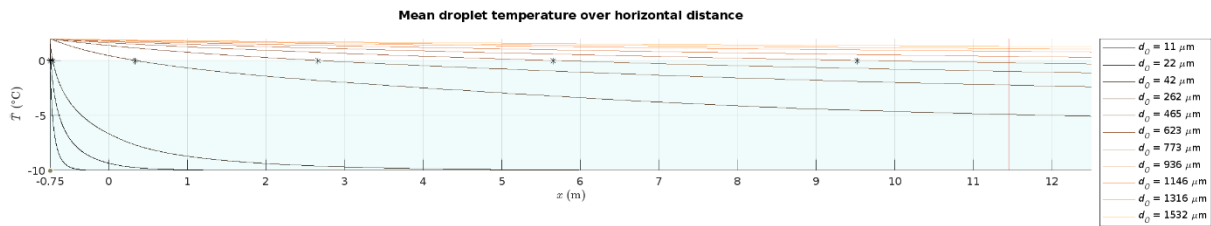


Figure 6: Results for a FZRA icing cloud simulation in the RTA IWT, the asterisks mark the position where the droplet reaches a supercooled state

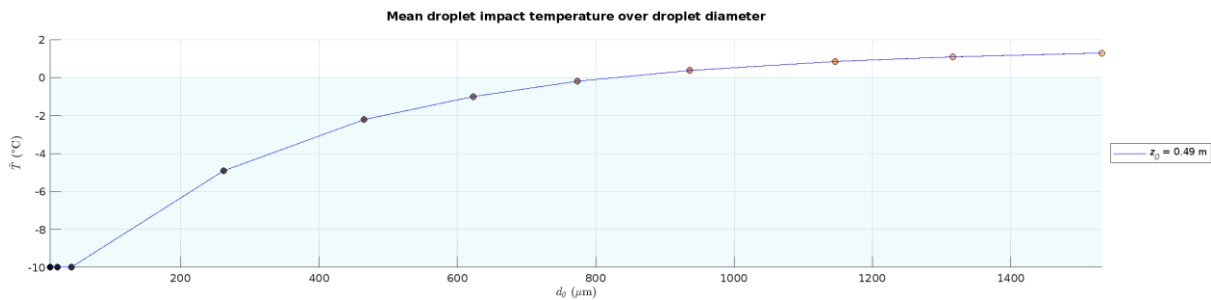


Figure 7: Mean droplet temperature in the test section (12.5m from the spray nozzles) at the RTA IWT

### 4.2.3 Droplet Temperature Validation

In order to validate the thermal droplet model, the numerical predictions were compared with experimental measurements. The measurements were only performed for FZDZ conditions. Therefore, same model was used to calculate the droplet temperature for a FZDZ MVD > 40 μm condition (at 60 m/s and a static air temperature of -5°C). In the numerical prediction, all droplets of the considered diameter spectrum cooled down at least to freezing temperature before reaching the test section. The mass averaged temperature for the particles of the large mode was about -4.1°C at the start of the test section according to the simulations.

Droplet temperature measurements have been performed by Rainbow Vision using their GRT-Mini instrument. The measurement has been performed with only the large mode of one of the FZDZ settings on both spray bar circuits active in order to increase the number of large droplets. The test

section airspeed was set to 60 m/s at a SAT of  $-5^{\circ}\text{C}$ . The measured water temperature in the spray nozzle supply lines was between  $5^{\circ}\text{C}$  and  $8^{\circ}\text{C}$ .

Figure 8 (left) shows a tri-modal Rosin-Rammler fit of the measured PSD, the measured MVD is in the region of  $140\ \mu\text{m}$ . In the right the recorded rainbow image from which the average temperature was derived is shown. An average droplet temperature of  $-4.1^{\circ}\text{C}$  was measured for the large mode of the FZDZ MVD  $> 40\ \mu\text{m}$  condition, which indicates a supercooled state of the large particles. This measurement confirms the numerically obtained results.

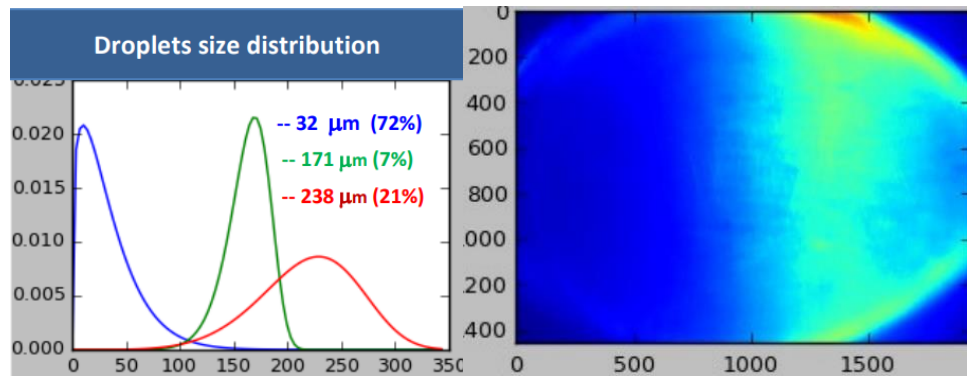


Figure 8: Example of validated measurement at RTA (for air temperature =  $-5^{\circ}\text{C}$ , air velocity = 60 m/s, fitted PSD (left), recorded rainbow image (right))

### 4.3 RTA Freezing Rain MVD > 40 μm Calibration

For Freezing Rain (FZRA) with a Median Volume Diameter (MVD) of larger than 40 μm, MVD, Particle size distribution (PSD) and Liquid Water Content (LWC) investigations have been performed during internal, nationally funded (“FFG Aviation Icing Tests II-IV” and “FFG AquaSense”) and internationally funded (“ICE GENESIS”) research projects. The Requirements on the PSD and the LWC range is shown in Figure 9.

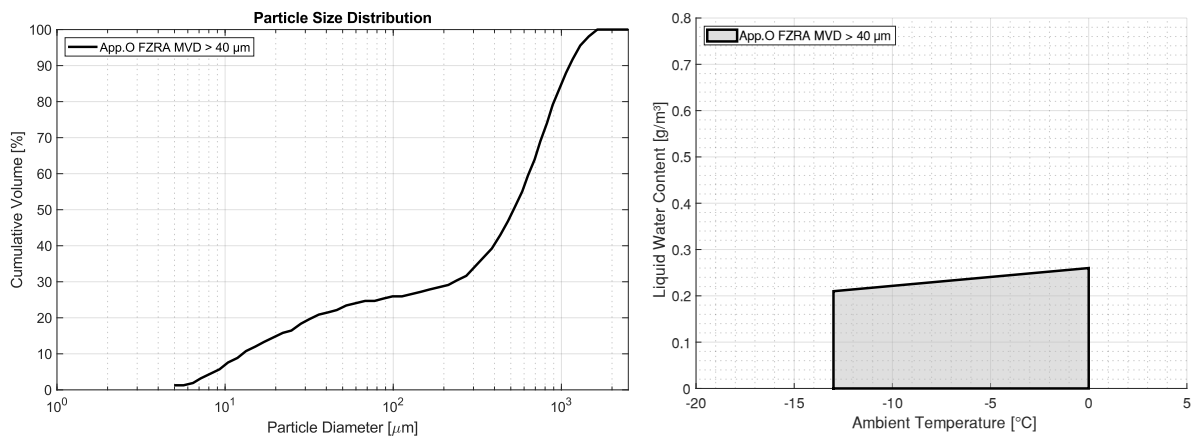


Figure 9: Appendix O Freezing Rain MVD > 40 μm PSD (left) and LWC range (right)

According to Cober and Isaac [1, p. 271] the MVD of FZRA MVD > 40 μm conditions should be in the range of 526 μm with a maximum diameter of 2229 μm. Figure 10 shows the individual measured PSDs and the average cumulative mass spectrum [2]. The 99.0% LWC of all cloud measurements was 0.26 g/m<sup>3</sup>, which is used as the upper limit in Appendix O, the maximum observed LWC was 0.41 g/m<sup>3</sup> [1, pp. 278-280].

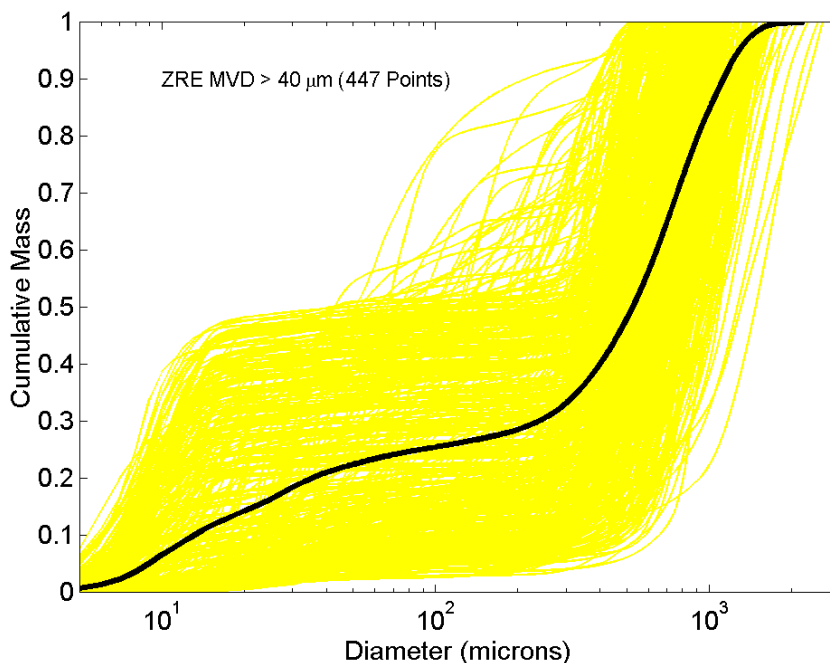


Figure 10: Average Cumulative Mass Spectrum for FZRA MVD > 40 μm compared to each individual cumulative mass spectra [2, p.45]

Based on preliminary investigations one main spray bar system setting emerged as the most promising one. This setting was investigated in more detail in the RTA IWT. Each of the eleven spray bars of the RTA spray bar system has two individually controllable circuits. This is used to create the required bimodal distribution for FZRA MVD > 40 μm. One circuit uses the standard atomizing nozzles, which

are also used for the generation of Appendix C conditions, the other circuit uses single medium nozzle to generate the large rain droplets. In order to improve the cloud uniformity, the spray nozzles for the large and small mode are arranged in an alternating pattern. To further improve the uniformity, the spray nozzles for the large mode are mounted on a slowly rotating body with a radius of about 140 mm.

#### 4.4 MVD / PSD Measurements

The MVDs and PSDs of the selected setting were measured using two different instrumentations, the Malvern Spraytec with the 750 mm lens assembly and a combination of the FCDP, 2D-S and PIP probe from Droplet Measurement Technologies, which was provided by DLR. MVDs between 350  $\mu\text{m}$  and 685  $\mu\text{m}$  were measured at different positions in the test section and different airspeeds. The detailed PSDs are shown in Section 4.4.2. Further information you will find under Ice-Genesis DEL D6.1 & D6.2 [3] and [9].

##### 4.4.1 MVD Calibration

Due to the bimodal nature of the FZRA distribution, the MVD was calibrated based on a combination of the small and the large mode. For the small Mode the standard Appendix C calibration curve was used. For the large mode, a separate calibration curve was created by fitting measurement data from Malvern Spraytec and Malvern Insitec measurements of individual single medium nozzles performed with the spray nozzle test rig. MVDs in a range between 600  $\mu\text{m}$  and 900  $\mu\text{m}$  were measured, depending on the spray nozzle water pressure. To derive the combined MVD of both modes, the LWC ratio calculated by the LWC calibration curves is used as shown in Equation 1.

$$MVD = MVD_s * \frac{lwc_s}{lwc_s + lwc_l} + MVD_{large} * \left(1 - \frac{lwc_s}{lwc_s + lwc_l}\right) \quad (1)$$

For the setting "FZRA L1" the calibrated MVD of the small mode is 19.8  $\mu\text{m}$ , the large mode has a calibrated MVD of about 718  $\mu\text{m}$ . According to Equation 1, this yields a combined MVD of 535  $\mu\text{m}$ . In Figure 11 a comparison between the calibrated and the measured MVDs can be seen. In the airspeed range from 45-70 m/s, the measurements fit within  $\pm 25\%$  of the calibration. At airspeeds of lower than 45 m/s and higher than 70 m/s a drop in the MVD was observed. Maximum particle sizes of up to 1550  $\mu\text{m}$  were measured in the test section. At the lower airspeeds this could be due to the gravitational influence, as the large droplets might impinge lower than the probe location. The same could be possible for the high airspeed, as the large droplets might pass over the relatively small probing area (at the vertical and horizontal centre of the test section area). Another explanation would be secondary droplet breakup occurring at the high airspeeds. In case of droplet breakup, an increased number of smaller particles would have been expected, which were not present in the measurement.

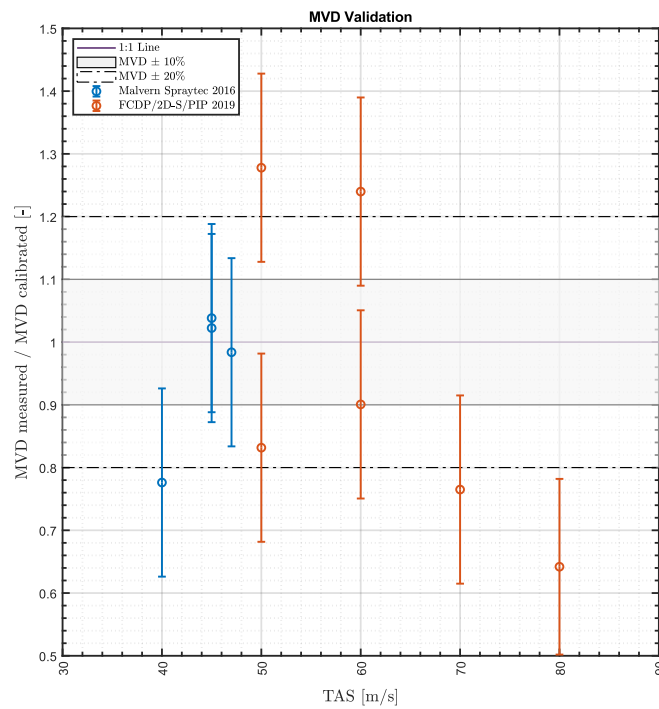


Figure 11: Comparison of calibrated and measured MVDs versus test section airspeed for FZRA MVD > 40 μm

#### 4.4.2 PSD Calibration

In addition to the MVD calibration, also a PSD calibration was derived, in order to predict the average PSD for different FZRA MVD > 40 μm settings. Figure 12, Figure 13 and Figure 14 show the measured distributions (left), on the right, q-q plots are shown, indicating the percentual deviation of the cumulative volume compared to the Appendix O requirement. Furthermore, a linear regression has been performed, the R<sup>2</sup> values are displayed in the legend. Overall, the measured PSDs were within ±10% to ±20% compared to the Appendix O distributions. The biggest deviations were observed for the measurements at 70 and 80 m/s. R<sup>2</sup> values of 0.830 to 0.994 were obtained with some distributions matching the requirements very well.

A single calibrated PSD was derived from the individual measurements. The calibrated PSD is based on a combination of two Langmuir distributions, which were generated using the calibrated MVDs for the small and the large mode. The cumulative volume is then recreated from the two distributions by using the ratio between the calibrated LWCs of the small and the large mode.

Figure 15 shows the resulting cumulative volume of the calibrated PSD (left) and a comparison with the Appendix O requirement for FZRA MVD > 40 μm (right). The calibrated PSD matches the requirement within ±10%. In Figure 16 and Figure 17, the calibrated and measured cumulative volumes are compared by means of q-q plots. A good agreement between the calibration and the measurement was achieved, indicating deviations of less than ±15%, up to 60 m/s, at higher airspeeds the deviation gets up to ±25%.

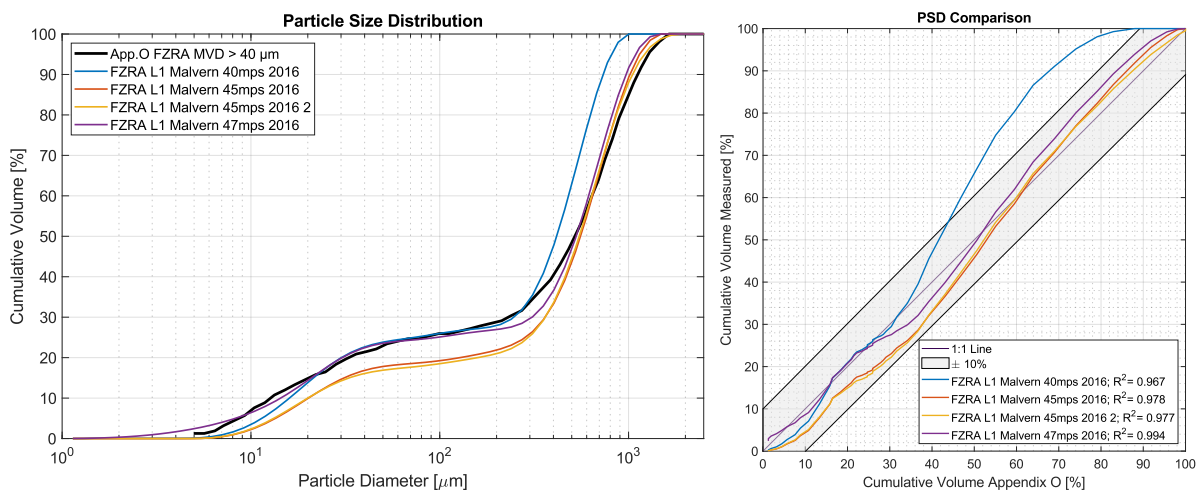


Figure 12: Measured PSDs for FZRA using the Malvern Spraytec compared to Appendix O requirements, cumulative volume (left), q - q plot (right); measurement performed at 2°C

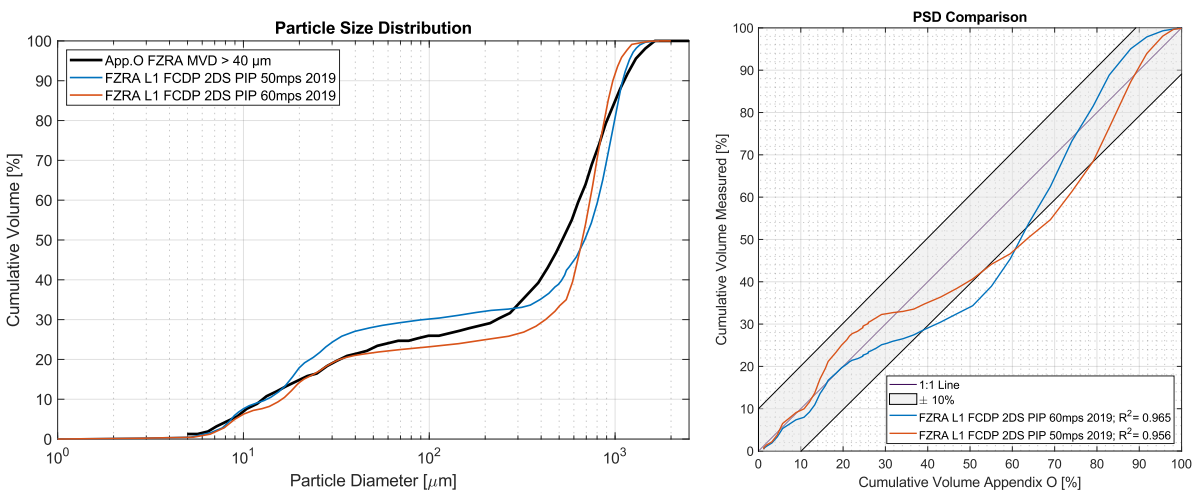


Figure 13: Measured PSDs for FZRA using the FCDP/2D-S/PIP combination compared to Appendix O requirements, cumulative volume (left), q - q plot (right); measurement performed at -5°C

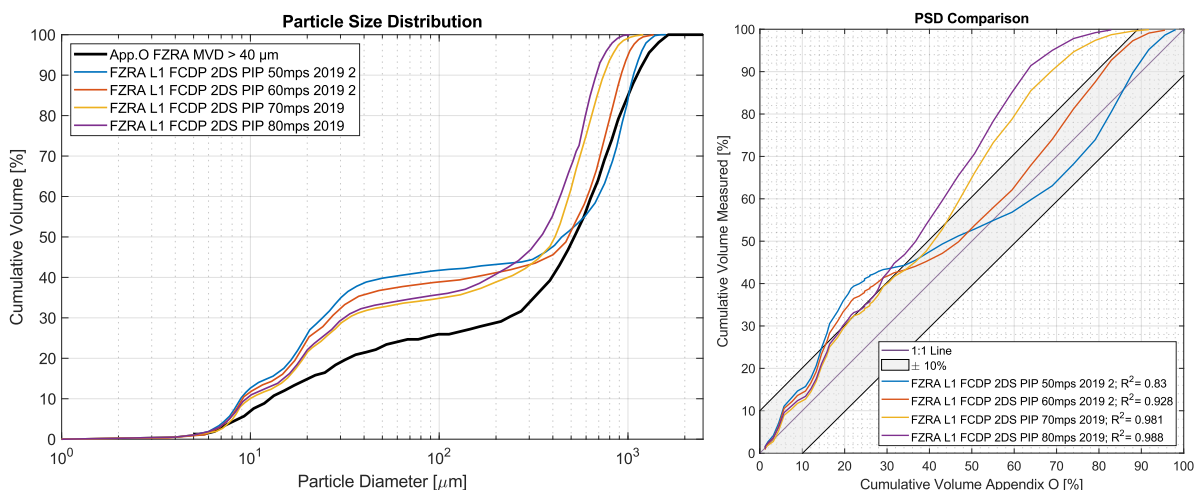


Figure 14: Measured PSDs for FZRA L1 using the FCDP/2D-S/PIP combination compared to Appendix O requirements, cumulative volume (left), q - q plot (right); measurement performed at 2°C

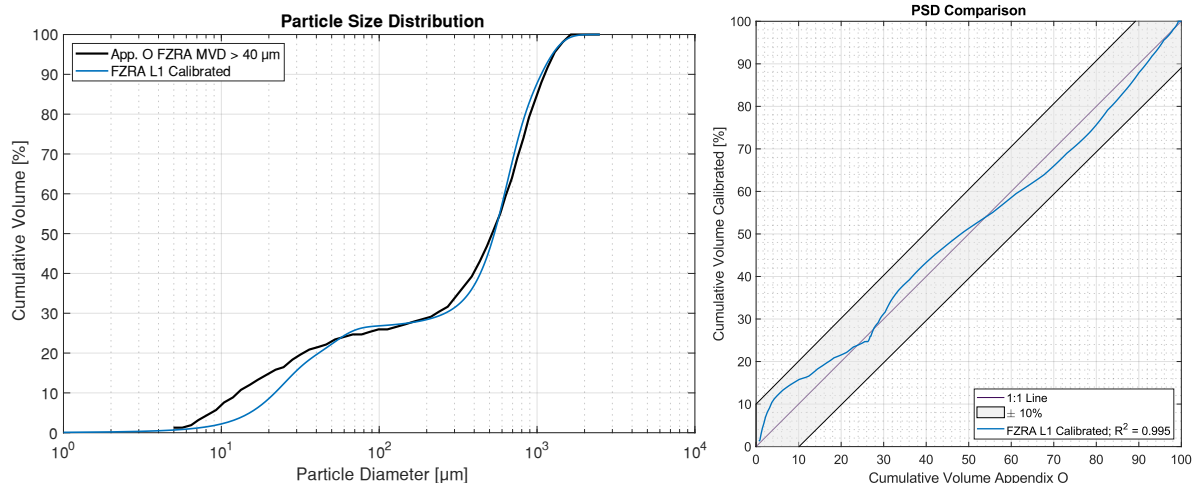


Figure 15: Calibrated PSD of FZRA L1 versus appendix O requirement, cumulative volume (left), q - q plot (right)

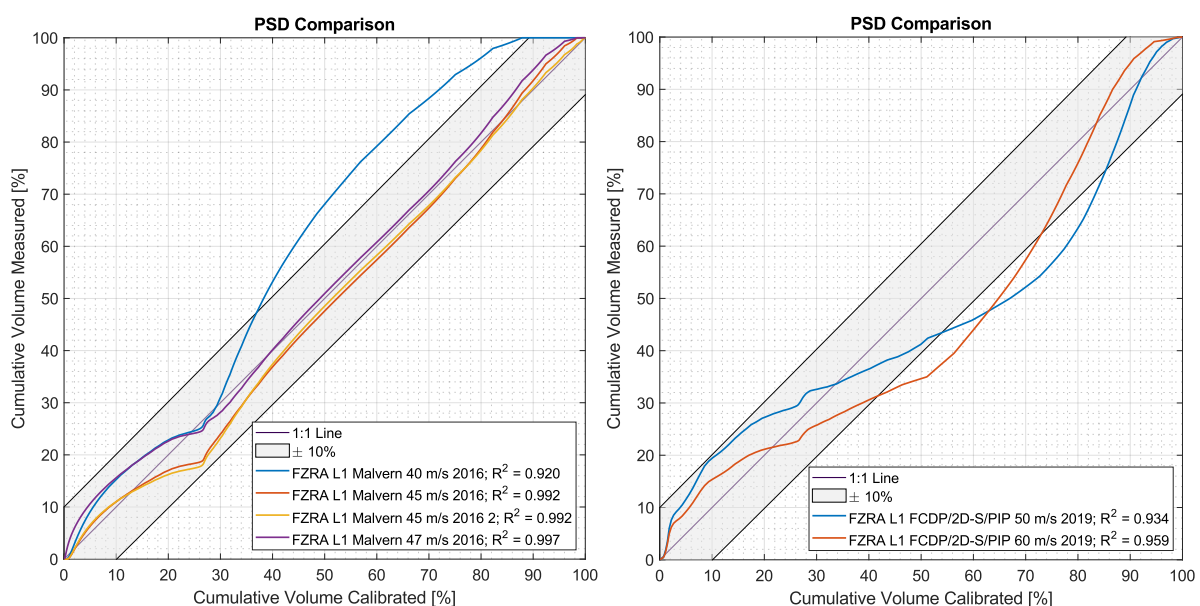


Figure 16: Comparison of measured cumulative volume versus prediction using the PSD calibration; Malvern measurements (left), FCDP/2D-S/PIP combination measured at -5°C (right)

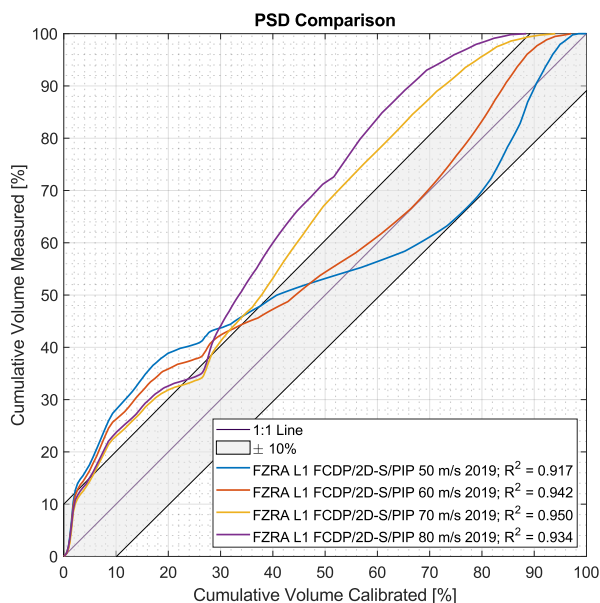


Figure 17: Comparison of measured cumulative volume versus prediction using the PSD calibration; FCDP/2D-S/PIP combination measured at 2°C

## 4.5 LWC Measurements

For the FZRA MVD > 40  $\mu\text{m}$  condition LWC measurements with the IKP from Cranfield University and a Nevzorov Probe (only 8 mm and 12 mm TWC element values were used) from DLR have been performed. Furthermore, the LWC has been estimated using the spray nozzle waterflows.

### 4.5.1 LWC Calibration

Similar to the MVD, the LWC calibration curve was also split into two parts, one for the small mode, which is equal to the standard LWC calibration, for the large mode no detailed calibration curve was derived, as LWC measurements were only made for one spray nozzle setting. Instead, the LWC for the large mode of “FZRA L1” was directly calculated based on the mean from the different measurement methods. As more data for the measurement of the full bi-modal distribution was available, the mean LWCs for the full FZRA condition were calculated for each instrument, the final LWC for the bi-modal distribution was then determined by taking the combined mean of the different instruments. To get the LWC of the large mode only, the calibrated LWC from the small mode was subtracted from the total LWC.

In Figure 18 a comparison between the measured and calibrated LWCs is shown for the full bi-modal distribution (left) and the large mode only (right). Overall, an agreement within  $\pm 25\%$  was observed, whereas the IKP is showing the highest water contents and the 8 mm Nevzorov Probe the lowest. Here it has to be noted, that the instruments were not mounted in the exact same position and the measurements were not performed within the same test campaign. Therefore, changes in the cloud uniformity could have influenced the result. Overall, the achievable calibrated LWCs were in the range of 0.25  $\text{g}/\text{m}^3$  to 0.40  $\text{g}/\text{m}^3$  depending on the airspeed.

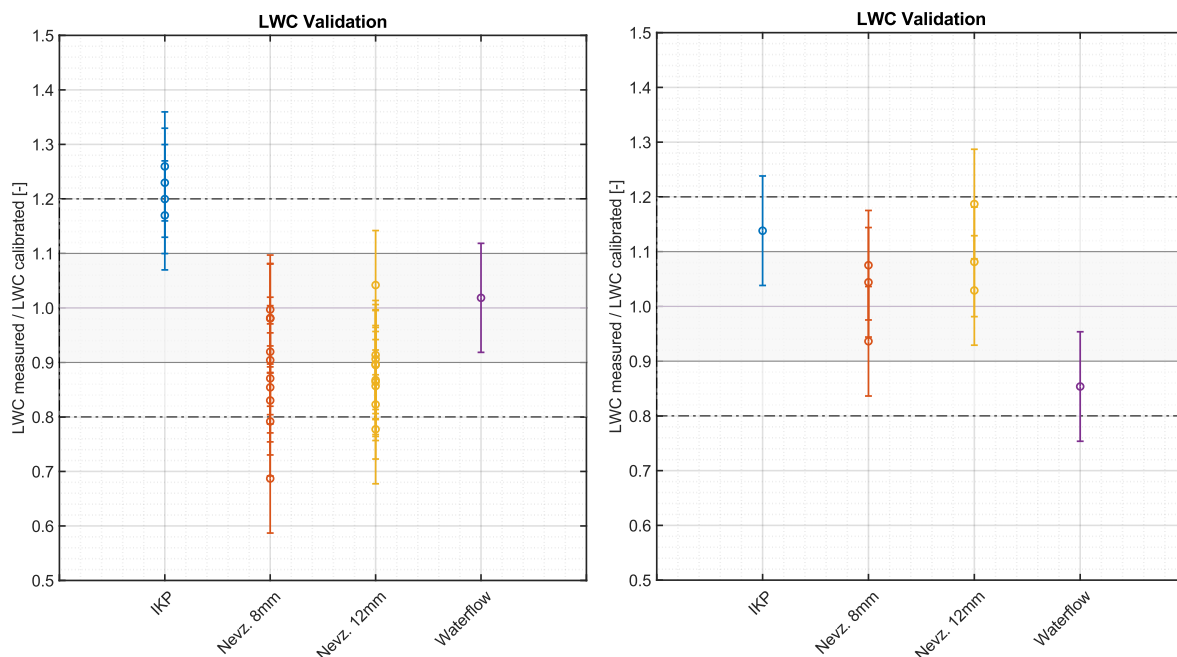


Figure 18: Comparison of calibrated and measured LWCs for FZRA MVD > 40  $\mu\text{m}$ , full bi-modal distribution (left), only large mode (right)

## 4.5.2 LWC Uniformity

The homogeneity and the overall extent of the FZRA MVD > 40  $\mu\text{m}$  cloud was investigated using the standard ice accretion grid. As the grid might not be able to fully capture the large rain droplets, the uniformity was also evaluated by means of ice accretion tests on a NACA0012 wing section. In order to increase the uniformity, the single medium nozzles are mounted on 3D printed rotating nozzle bodies. For the grid measurement only three spray bars were equipped with a total of 22 “SLD” nozzles. The resulting uniformity can be seen in Figure 19. An acceptable uniformity ( $\pm 20\%$ ) was achieved over an area of about 1  $\text{m}^2$  (2.1 m x 0.48 m).

Since the grid should only be used as a qualitative means to assess the rough coverage area, also ice accretion tests on a NACA0012 wing section were performed. The resulting ice shapes were documented by means of high-resolution 3D scans. For the investigation with the NACA0012 wing section the SLD spray nozzle configuration was extended to a total of 30 (mounted on four spray bars), which should extend the uniform area vertically. Some further improvements to the uniformity were made by pre-selecting spray nozzles based on water flow rate tests in the spray nozzle test rig. Furthermore, the stability and consistency of the rotating nozzle mechanism was improved, which resulted in a better overall cloud uniformity compared to the grid measurement. Figure 20 shows Photographs of a 10-minute FZRA MVD > 40  $\mu\text{m}$ , at a test section airspeed of 60 m/s and an ambient temperature of  $-5^\circ\text{C}$ . The “FZRA L1” setting was used, which has a calibrated MVD of 536  $\mu\text{m}$  and a calibrated LWC of about 0.34  $\text{g}/\text{m}^3$ . The observed accretion was uniform over the whole 1.8 m span of the wing section. The impingement limits also were constant over the whole span, indicating a uniform particle size distribution. On the stagnation line the ice thickness stayed within  $\pm 10\%$  over the whole span.

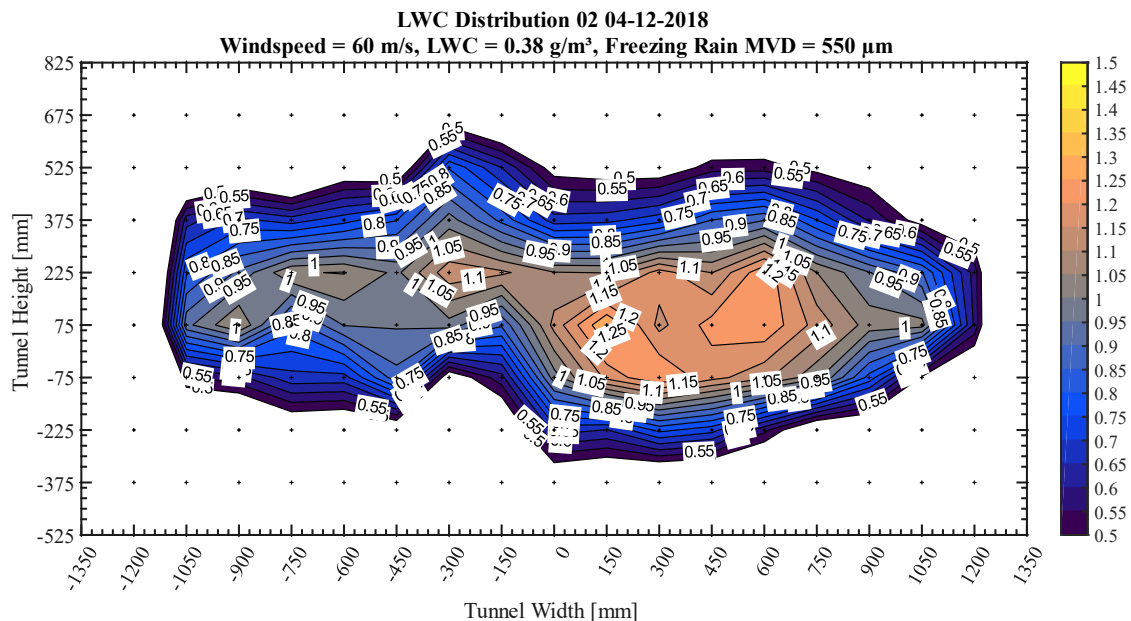


Figure 19: LWC Uniformity for “FZRA L1” at a test section airspeed of 60 m/s, measured using the ice accretion grid, in total 22 “SLD” Nozzles were used

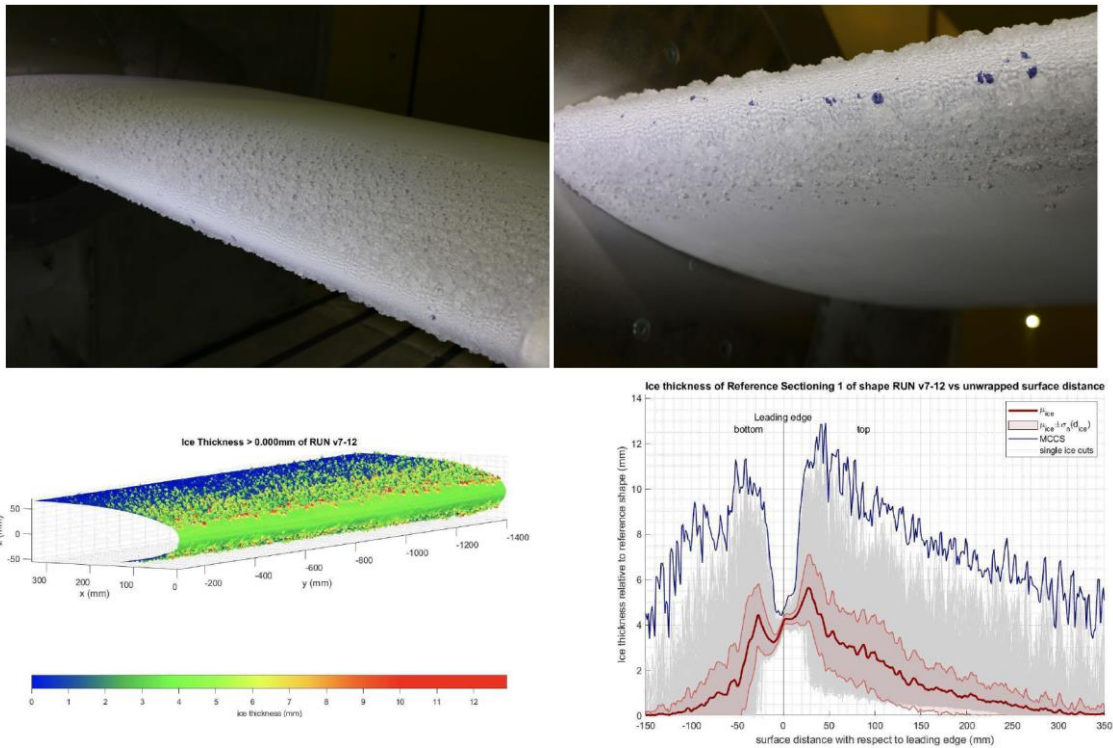


Figure 20: Photographs of a FZRA MVD > 40 μm ice accretion (Setting "FZRA L1"), TAS = 60 m/s, SAT = -5°C, exposure duration = 600s

### 4.6 RTA FZRA Envelopes

The capability of generating FZRA at RTA was assessed in detail and potential limitations were found and have been evaluated. In Figure 21 and Figure 22 the resulting FZRA envelopes for the RTA IWT are shown. Detailed measurements have only been performed for one setting. The calibrated PSD is very close to the Appendix O requirement. At higher speeds (> 70 m/s) the distribution might change slightly, but more measurement data is required to fully characterize the FZRA cloud over the whole test section area and airspeed range. The achievable LWC for the FZRA condition depends on the airspeed, at 80 m/s the calibrated LWC is 0.25 g/m<sup>3</sup> and at 50 m/s (the lower speed limit for this condition) the calibrated LWC came out as 0.40 g/m<sup>3</sup>.

Numerical simulations have shown that the droplet trajectory angles, and droplet velocities are very close to the ambient conditions. Secondary droplet breakup for particles up to about 1500 μm should also not be a significant issue. When injecting the water at cold enough temperatures, the droplets also get within 10°C compared to the ambient temperature.

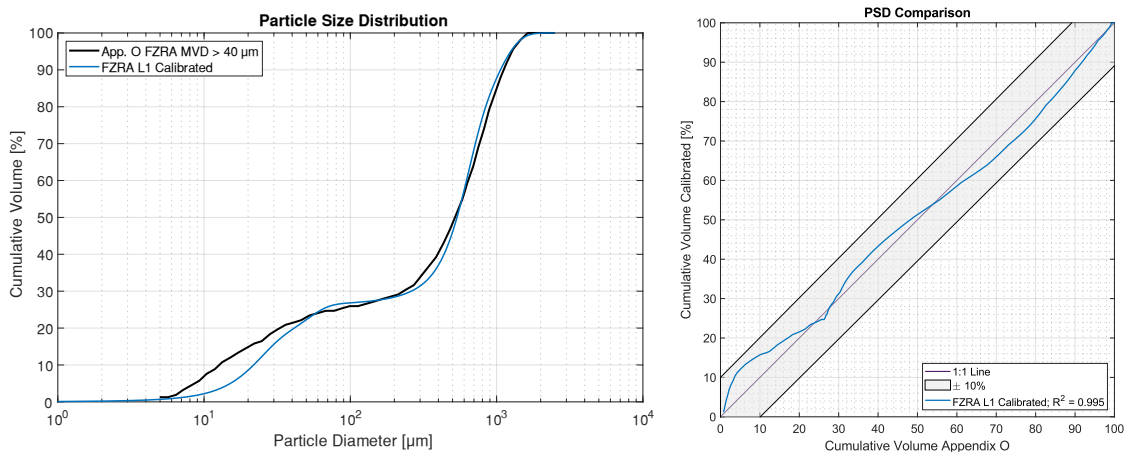


Figure 21

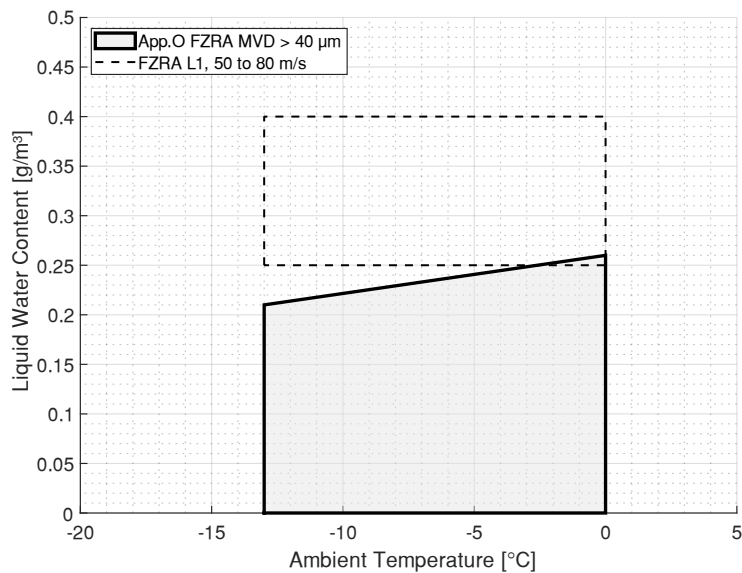


Figure 22

## 5 CIRA-IWT Assessment

The main focus for the CIRA-IWT was to characterize the FZDZ envelope in the function of the matrix of conditions defined for the ice accretion campaign foreseen in the project on the 3D wing specimen. Therefore, there was no dedicated FZRA assessment during the unique available measurements slot where the set of instruments selected was focused only on FZDZ clouds, although some cloud conditions showed potential FZRA features in their spectra.

### 5.1 CIRA-IWT layout and main features

This facility has three interchangeable test sections and one open jet configuration. The aero-line with main internals and configurations is shown in Figure 23 with a table summarizing main performances. Some features are still unusual for large icing wind tunnel: downstream the fan diffuser, a twin row heat exchanger is also capable to control the air Relative Humidity (RH) before the spray bar, by means of a hot air compressor and steam injection. Controlled humidity ranges between 70% and 100% for temperatures between  $-15^{\circ}\text{C}$  and  $-20^{\circ}\text{C}$ . 100% humidity value can be set between  $-20^{\circ}\text{C}$  and  $-40^{\circ}\text{C}$ . Control accuracy is within  $\pm 5\%$  RH.

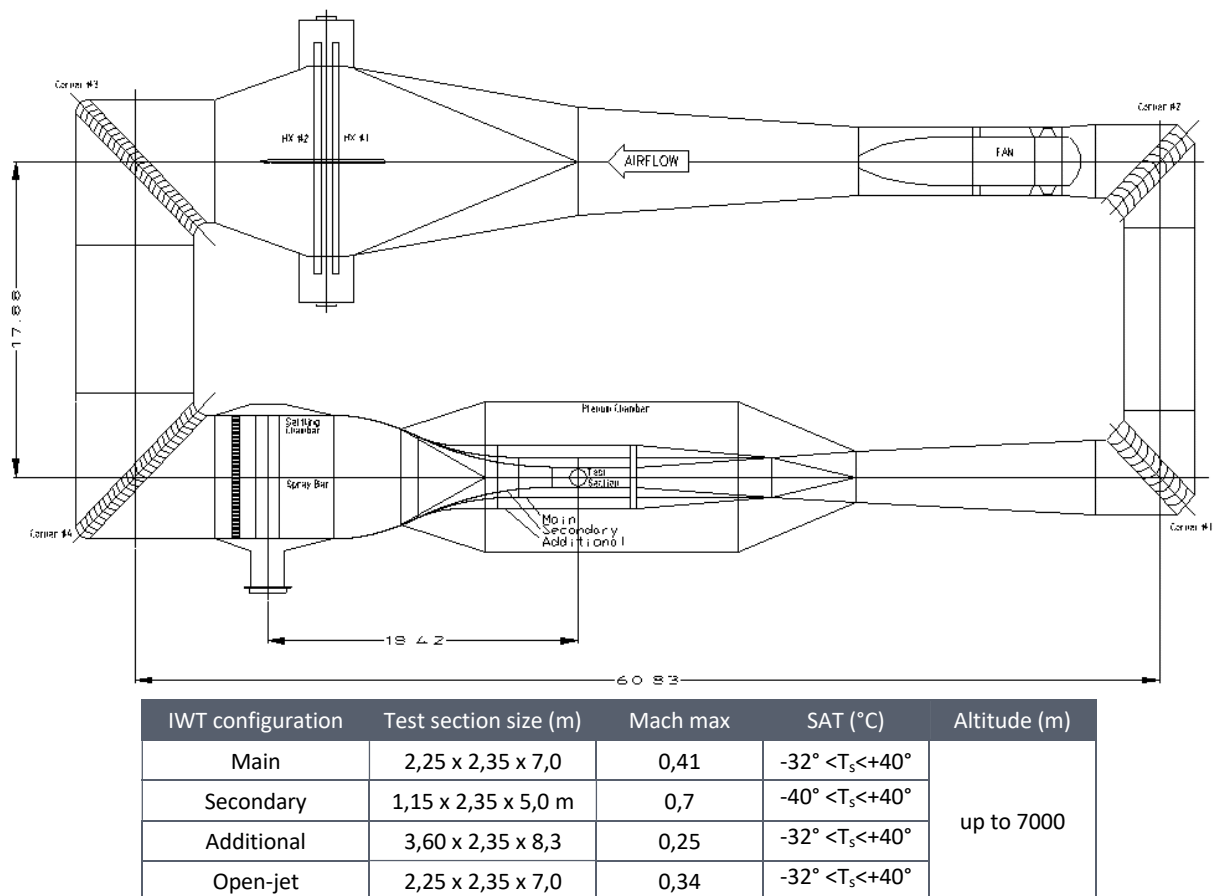


Figure 23: CIRA Icing Wind Tunnel layout with main information on the test section configurations and performance

The facility settling chamber is fitted with a honeycomb module to reduce large scale eddies thus ensuring flow straightening. Downstream the honeycomb, an interchangeable section provides the possibility to switch the spray bar module with the screens module to improve the flow quality in the test section allowing the execution of the aerodynamic tests. A 0.7 MW centrifugal compressor unit

allows the pressure to be regulated between 0.39 bars (corresponding to an altitude of 7000 meters) and 1.45 bars. While depressurization is used to simulate altitude for icing tests, pressurization, combined with a reduction in air temperature, helps to increase the Reynolds number for aerodynamic tests.

### 5.1.1 Preliminary assessment of FZRA with MVD > 40 $\mu\text{m}$ in CIRA-IWT

The assessment of the FZRA condition was limited by the measurement's objective with the main focus to address the CIRA SLD calibration for the FZDZ cloud conditions. To this end, the definition of the PSD instrumentation is based on probes with sampling volume limited to better characterize the FZDZ. DLR supports this part of the calibration by providing the CCP probe (Figure 24), which is a combination of scattering technique, CDP with a 2  $\mu\text{m}$  – 50  $\mu\text{m}$  size range, and CIP-G probe, an Optical Array Probe with a 15  $\mu\text{m}$  – 930  $\mu\text{m}$  size range.

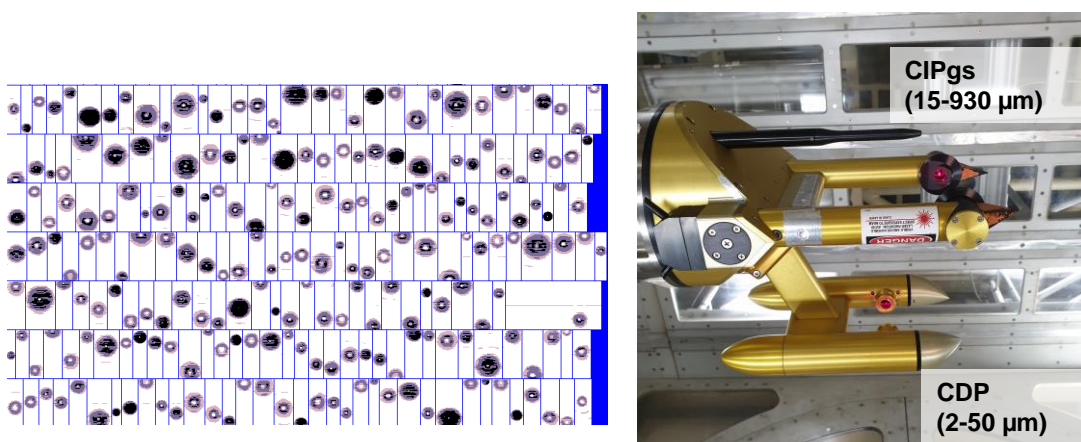


Figure 24: DLR CCP (Cloud Combination Probe) installed in the centerline of the CIRA IWT test section during the PSD/MVD measurement slot. The picture on the left shows the droplet images with diameters higher than 100  $\mu\text{m}$

For some of the spray conditions collected with this instrument, results of PSD/MVD measurements shows potential lack of mass for the large size bin in the spectra as reported in the Figure 25. In this case with 130  $\mu\text{m}$  of MVD and nominal 0.24  $\text{g m}^{-3}$  of LWC (no hot-wire data are available for that condition), the concentration rolling-off at 450  $\mu\text{m}$  of size diameter starting from a value close to  $10^7 \text{ m}^{-4}$  which represents the number concentration density of particles with this diameter (see Figure 25). This behaviour shows a suspect lack droplets statistic for the CIP-GS due to its limited sampling volume. Potential particle statistical issue seems starting from 320  $\mu\text{m}$  representing the max size diameter in the mass distribution plot. Indeed, the unsymmetrical bell shape in this plot suggest potential presence of low droplets concentration with a larger diameter in the cloud.

Additional effort to characterize FZRA could be performed in the future calibration of CIRA-IWT involving instruments like PIP (Precipitation Imaging Probe) with 50  $\mu\text{m}$  of resolution and max measurable diameter of 3200  $\mu\text{m}$ .

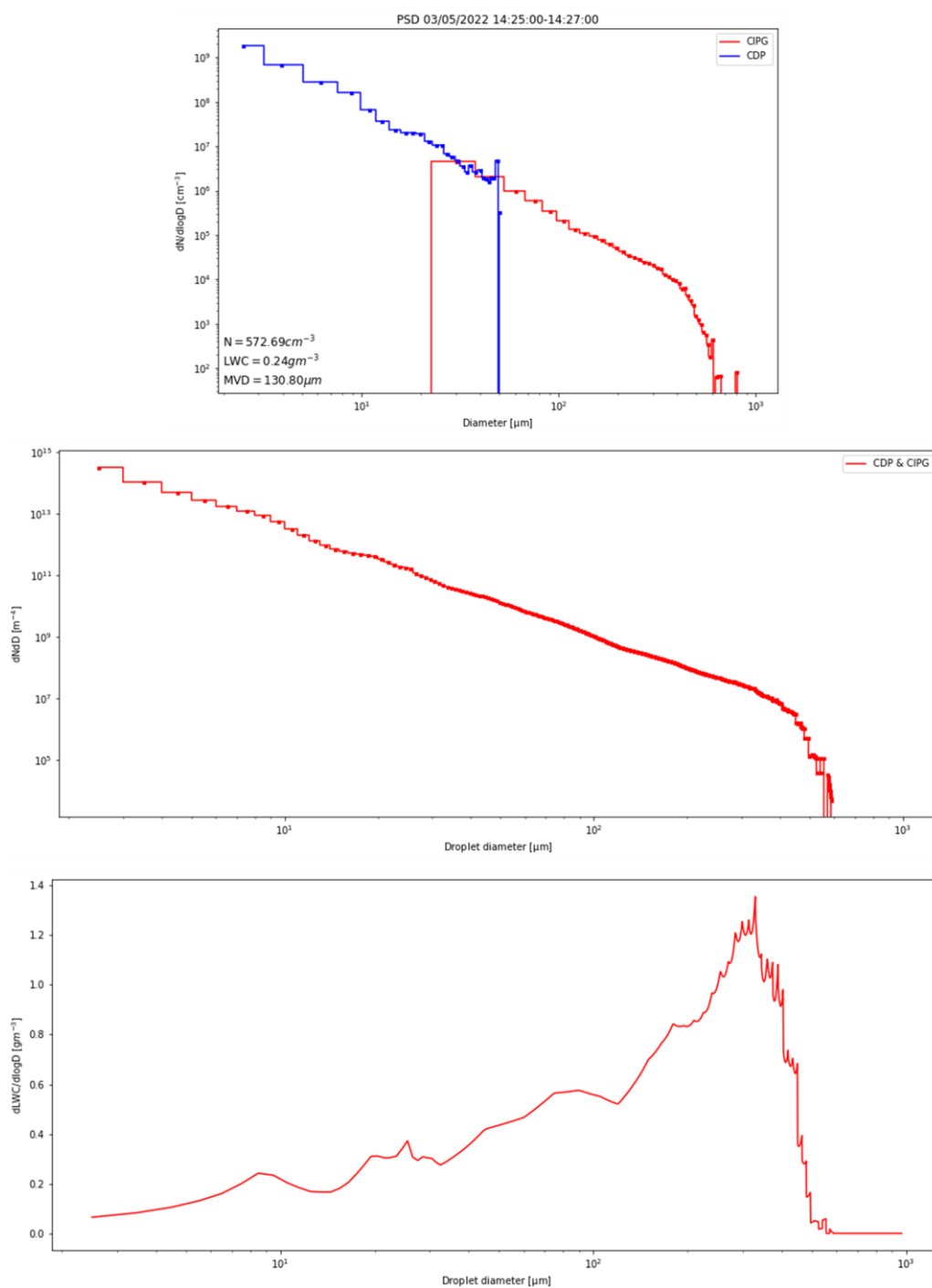


Figure 25: Typical plots representing some of the cloud conditions collected during the CCP measurements. In this particular case, the data have been collected at 110 m/s with airstream temperature at  $-6^\circ\text{C}$  and pressure altitude representing 6,096 m. The plot on the top represents the combination of the concentration measured by each sensor (CDP+CIP-Gs); the plot in the middle number concentration density of particles in function of diameter  $D$ ; the plot on below shows the mass distribution for the combined PSD.

## 6 Conclusion

---

The performed measurements, investigations and calibrations have shown that the RTA IWT can produce Appendix O conditions (FZDZ MVD < 40  $\mu\text{m}$ , FZDZ MVD > 40  $\mu\text{m}$  and FZRA MVD > 40 $\mu\text{m}$ ) close to the requirements. The main limitations are the relatively high-water contents which are required to match the bimodal PSDs in FZDZ and FZRA. This also limits the variability of the producible conditions as the LWC is mainly influenced by the test section airspeed. Ice accretion tests and droplet temperature measurements have shown that the large droplets are sufficiently supercooled at temperatures of colder than -5°C. Further testing is required to investigate if that is still the case at warmer temperatures.

A few test campaigns with FZDZ and FZRA conditions have already been performed and further validation and testing is planned in upcoming research projects. Especially the FZRA setup is still in a prototype stage and needs further improvement to be more practical in a testing environment.

Following the commissioning of the CIRA-IWT spray bar system equipped with the new spray nozzle, the available measurement slot (April 2022 - June 2022) allowed for characterizing the SLD clouds limited to the FZDZ conditions mainly focused on the ice accretion campaign for the 3D wing test article. The ability to generate the FZRA conditions has not been evaluated for the exclusion between the used instruments of a specific imaging probe with an appropriate larger sampling volume and higher optical resolution (> 50  $\mu\text{m}$ ), limiting the detection of large droplets. Nevertheless, indications provided by DLR-CCP allow in suspecting the presence of larger droplets for some spray bar conditions that can be figured out as potential capability in generating FZRA in CIRA-IWT that might be further investigated in a future program.

## 7 References

---

- [1] Cober, S. G., and G. A. Isaac, 2011: "Characterization of Aircraft Icing Environments with Supercooled Large Drops for Application to Commercial Aircraft Certification," *Journal of Applied Meteorology and Climatology*, Volume 51, pp.265-284, <https://doi.org/10.1175/JAMC-D-11-022.1>
- [2] Federal Aviation Administration FAA, 2009: "Data and Analysis for the Development of an Engineering Standard for Supercooled Large Drop Conditions", DOT/FAA/AR-09/10, National Technical Information Services (NTIS), Springfield, Virginia 22161
- [3] Ice-Genes public deliverable D6.1 & D6.2: "Proposal of Calibration Instruments and Procedures for FZDZ and FZRA "
- [4] King, M.C., Bachalo, W.D., Bell, D. and King-Steen, L.E., "Weber Number Tests in the NASA Icing Research Tunnel", AIAA
- [5] Clift, R., Grace, J. R., and Weber, M. E., *Bubbles, Drops and Particles*, Dover Publications, Inc., Mineola, 2005
- [6] Salman, A. D., and Verba, A., "New Approximate Equations to Estimate the Drag Coefficient of Different Particles of Regular Shape," *Periodica Polytechnica of the Technical University Budapest - Chemical Engineering*, Vol. 32,1988
- [7] Wierzba, A., "Deformation and breakup of liquid drops in a gas stream at nearly critical Weber numbers," *Experiments in Fluids* Vol. 9, pp. 59-64, 1990
- [8] Fallast, A., Rapf, A.R., Tramposch, A. et al. "Kinetic and thermal simulation of water droplets in icing wind tunnels". *CEAS Aeronautical Journal* 13, pp. 181–198 (2022). <https://doi.org/10.1007/s13272-021-00558-y>
- [9] Breitfuss, Wolfgang. 'WP6 SLD TEST CAPABILITY RTA CALIBRATION RESULTS'. Presented at the ICE GENESIS Public Workshop, Vienna, 2022. [https://www.ice-genesis.eu/media/articles/files/2nd\\_Public\\_Workshop/ICE\\_GENESIS\\_Public\\_Forum\\_RTASLD\\_Test\\_CAPABILITY\\_R1.0.pdf](https://www.ice-genesis.eu/media/articles/files/2nd_Public_Workshop/ICE_GENESIS_Public_Forum_RTASLD_Test_CAPABILITY_R1.0.pdf).